Earth and Planetary Science Letters 335–336 (2012) 88–94

Contents lists available at SciVerse ScienceDirect

Earth and Planetary Science Letters

journal homepage: www.elsevier.com/locate/epsl

A 'continuity-index' for assessing ice-sheet dynamics from radar-sounded internal layers

Nanna B. Karlsson [a,b,*], David M. Rippin [c], Robert G. Bingham [d], David G. Vaughan [b]

[a] Department of Geography, University of Hull, UK
[b] British Antarctic Survey, Cambridge, UK
[c] Environment Department, University of York, Heslington, York, YO10 5DD, UK
[d] School of Geosciences, University of Aberdeen, Aberdeen, AB24 3UF, UK

ARTICLE INFO

Article history:
Accepted 23 April 2012
Editor: T.M. Harrison

Keywords:
glaciology
radio-echo sounding
internal layers
West Antarctica
ice-penetrating radar
ice dynamics

ABSTRACT

Radio-echo sounding (RES) of polar ice sheets reveals extensive internal layering. The degree of continuity of internal layering holds critical information about the ice-flow field, but previous analyses of this parameter have been limited to qualitative classifications. Here we present a new quantitative method for analyzing internal layer continuity—named the continuity-index. When applied to data from Pine Island Glacier, West Antarctica, the new method clearly identifies a continuum of discontinuity of internal layers that corresponds with the current ice-velocity field. The analysis provides further support that the main trunk and tributaries are unlikely to have undergone substantial migration since the deposition of the internal layering. Significantly, our new method for analyzing internal layers is readily transferable across RES datasets, offering promise for data-led assessments of past and present flow dynamics across large areas of Antarctica and Greenland.

1. Introduction

Radio-echo sounding (RES) is the principal method by which the subsurface properties of polar ice sheets are investigated. While a typical focus for data acquisition is basal topography (e.g. Drewry, 1983; Vaughan et al., 2006), of increasing interest are the numerous internal layers that RES reveals within the ice (e.g. Fujita et al., 1999; Catania et al., 2005, 2010; Leysinger Vieli et al., 2011). Internal layers represent changes in the dielectric properties of ice with depth, likely induced by changes in density, acidity or crystal-fabric orientations. The layers that are imaged by RES typically result from constructive interference formed by radio-wave reflections off several parallel and closely spaced dielectric interfaces, and it is generally agreed that they are isochrones (Siegert, 1999; Miners et al., 2002; Matsuoka et al., 2003; Hindmarsh et al., 2009). In any location, isochrone stratigraphy results directly from the combined influences of mass balance and ice flow, hence, patterns of internal layering can store information about the past behavior of an ice mass (Jacobel et al., 1993; Leysinger Vieli et al., 2007).

In several earlier studies, the geometry of internal layering has been mapped across parts of Antarctica to investigate the past dynamics of ice streams and tributaries, and glean information about their spatial and temporal stability (Siegert et al., 2003; Rippin et al., 2003, 2006; Bingham et al., 2007). This method classifies the radar data according to the degree of layer disruption and, while useful, it is inherently limited by its reliance on manual assessments of layering type, which are time-consuming to carry out, and potentially subjective in their implementation. Here, we offer a significant advancement through the development of a new quantitative method for the classification and mapping of internal layers imaged in RES data, optimized to work with raw, digital radar traces, and thereby transferable across RES datasets. We apply the method to RES data acquired over Pine Island Glacier (PIG), West Antarctica and interpret the results in terms of past and present flow dynamics.

2. Data and methods

In this study, we make use of the data acquired by the RES system PASIN (Polarimetric Airborne Survey INstrument) over PIG during a collaborative UK/US survey in the austral summer of 2004/05 (Vaughan et al., 2006). We only use data from flights that were carried out at a constant distance above the ice surface comprising approximately 4900 km of survey lines. The radar system was operated with a transmit power of 4 kW around a

* Corresponding author. Present address: Centre for Ice and Climate, Niels Bohr Institute, University of Copenhagen, Juliane Mariesvej 30, 2100 Copenhagen, Denmark. Tel.: +45 35364289.
E-mail address: nanna.karlsson@nbi.ku.dk (N.B. Karlsson).

0012-821X/$ - see front matter © 2012 Elsevier B.V. All rights reserved.
http://dx.doi.org/10.1016/j.epsl.2012.04.034

central frequency of 150 MHz. The bed was sounded with a 4 μs 10 MHz chirp pulse. Post-processing of onboard-aircraft GPS measurements gives a positional accuracy better than ±1 m. The full dataset comprises individual data pulses, or traces, at a typical spacing of 15–30 m. Further information about the wider survey objectives and the radar instrumentation is provided by Vaughan et al. (2006) and Corr et al. (2007).

RES data are typically presented in two formats: as a plot for each trace (A-scope; Fig. 1a, c) and as an image comprising a series of adjacent traces (Z-scope; Fig. 2a–c). Some previous studies (e.g. Siegert et al., 2003; Rippin et al., 2003, 2006; Bingham et al., 2007) have classified internal layering manually by looking at the Z-scope images and determining whether sections of the Z-scopes possess one of the three types of layering: (1) well-preserved, or continuous layers (Fig. 2a); (2) disrupted or discontinuous layers (Fig. 2b); and (3) absent layers (Fig. 2c). Often a high correlation between layer type and ice velocity is observed; continuous, undisturbed layers are typically observed in slow flowing areas while faster flowing areas often contain disrupted layering. Areas that do not exhibit this correlation, and in which observed layer patterns differ from the currently active processes, have been interpreted as representing relict flow features (e.g. Rippin et al., 2003).

In the above examples, the 'manual' methodology was imposed by the analogue nature of the datasets used (1970s SPRI-NSF-TUD data; see Siegert, 1999). However, the digital nature of modern RES acquisition, exemplified by the PIG dataset, offers an opportunity to reconstruct the methodology quantitatively, thus removing the requirement for potentially subjective classification of internal-layering types.

Our method works directly from A-scope records, each trace representing a stack of ten consecutive raw traces (to minimize noise), but otherwise unprocessed (Fig. 1a, c). The lack of processing is deliberate—it reduces any dependence on filtering, migration or background removal operations that can introduce further subjectivity or modification/loss of data (e.g. Hubbard and Glasser, 2005) and it optimizes transferability of the method to other digital RES datasets. We next discard the upper and lower fifths of the ice column in each A-scope record, because no layers are visible in these parts of the radar signal. This is because the upper part of the ice primarily contains signals from density differences that the chirped PASIN signal does not resolve well (H. F. J. Corr, pers. comm., 2009), while the lower ice typically contains no internal layering (cf. Drews et al., 2009). Thus any signals in the upper and lower fifths of the ice will most likely not be the result of internal layering, and are therefore removed from consideration. Test results were generated omitting the upper and lower 10% and 5% of A-scopes instead and showed little to no change, with the only notable difference being a slight decrease in sensitivity to layer changes due to additional noise.

Internal layers are represented in each A-scope record as peaks of high reflected relative power bounded by values of lower reflected relative power, since a layer is, in essence, a boundary of high dielectric contrast. A-scope plots from regions of ice containing numerous internal layers thus fluctuate between extreme low and high values—in other words, they exhibit high-amplitude fluctuations (e.g. Fig. 1a). By contrast, in regions where internal layers are less clear or absent, radar waves will pass through fewer boundaries of high dielectric contrasts, with any boundaries encountered most likely caused by, for example, single scattering objects in the ice, or signal noise. Thus, the A-scope plots from regions where few layers are resolved will still show oscillating signals but these will be less frequent and of a smaller amplitude (Fig. 1c). The main difference between the two cases (in a single A-scope trace) will therefore not be the overall range of reflected relative power but rather the rapidity with which the signal changes between extreme low and high values. This can be quantified by considering the gradient of each A-scope plot. For each A-scope, we derive a continuity-index ψ, the mean of the absolute value of the derivative. In other words, if the total number of reflected relative power values between surface and bed rock is M we define a sub-interval with N values $[(1+M/5) : (M-M/5)] = [n_1 : n_N]$ and then ψ is calculated as:

$$\psi = \frac{1}{2\Delta r N} \sum_{i=n_1}^{n_N} |P_{i+1} - P_{i-1}| \quad (1)$$

where P_i is the reflected relative power (dB) at point i and Δr is the depth (m). Since the changes in ψ across the dataset are of much more interest than the actual value of ψ, the depth term

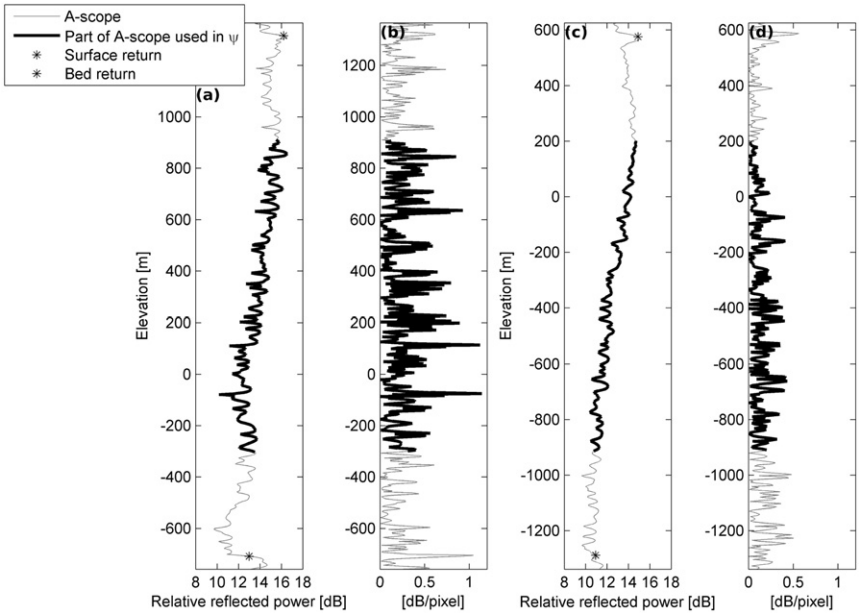

Fig. 1. (a) A-scope plot from an area containing numerous, internal layers (corresponding to the black line in 2a), (b) The absolute value of the gradient of (a) (c) A-scope plot from an area containing few internal layers (corresponding to the black line in 2c), (d) The absolute value of the gradient of (c).

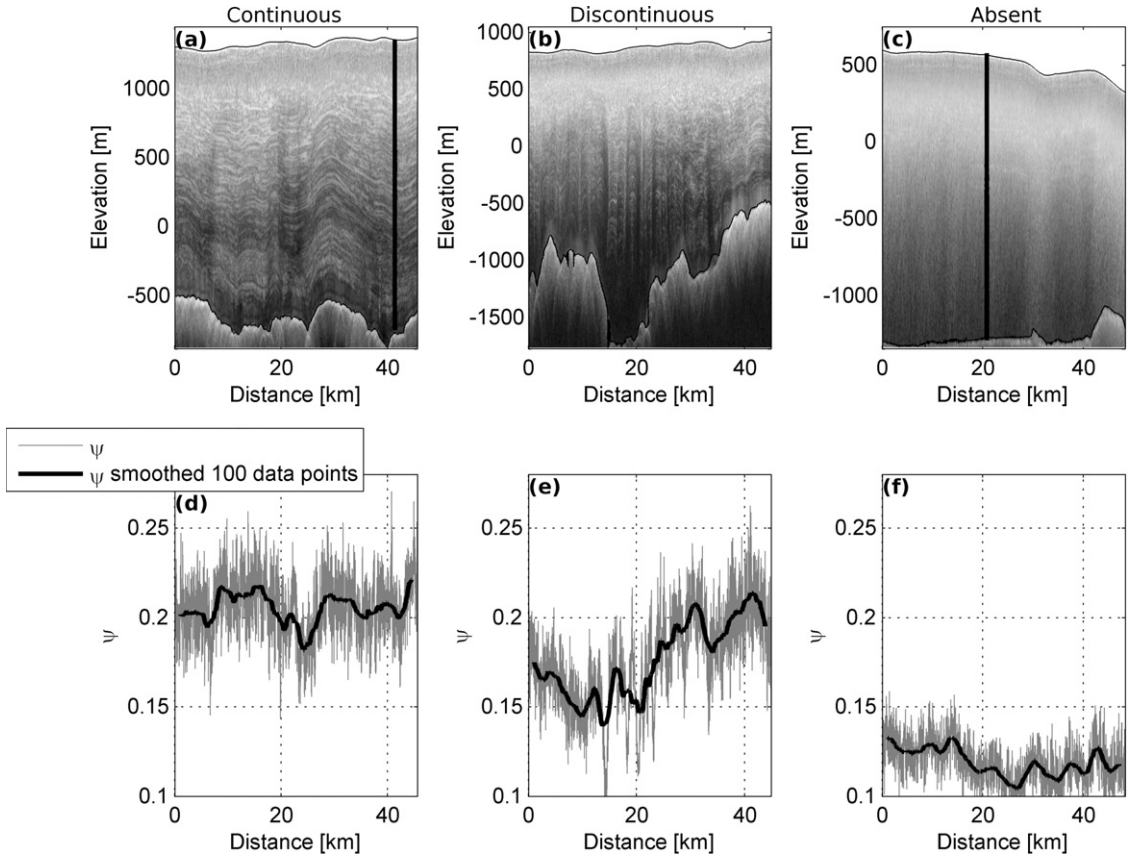

Fig. 2. Z-scope images from PIG showing from (a) continuous, (b) discontinuous and (c) absent layering. The black lines mark the surface and bed reflections. The location of the data is indicated in Fig. 3b. (d–f) The continuity-index ψ of the A-scopes shown in (a–c) (gray line) with a running mean of 100 traces (black line).

essentially works as a scaling factor and is here set equal to 1. For the same reason ψ is considered to be dimensionless although strictly speaking it has dimensions dB/depth.

In essence, A-scopes from areas with clear internal layers return a high continuity-index, whereas A-scopes interrogated where layering is absent return a low continuity-index. To assess overall layer continuity along flightlines, we average the continuity index over horizontal windows of 100 traces and 1000 traces, corresponding to 1–2 ice thicknesses ($\approx$3 km) and ten ice thicknesses ($\approx$30 km). Hence, flightline sections characterized by 'well-preserved' layers return consistently high continuity-indices because consecutive traces will all have high continuity indices; conversely, sections with largely absent layering return the lowest continuity index (low continuity-indices). Flightline sections characterized by discontinuous layers, i.e. regions that indicate present or previous enhanced flow, are qualitatively characterized by layer packages interspersed with regions of little to no layering (Fig. 1b), so that, along-track, continuity-indices for individual A-scope range from high to low (Fig. 1e). Consequently, over any smoothing window (e.g. 100 traces, 1000 traces) in such regions an intermediate value is returned.

3. Results from Pine Island Glacier

We now present the results of the method applied to radar data from Pine Island Glacier, one of the largest and most dynamic glacial basins of West Antarctica (Wingham et al., 2009). The northern part of the basin contains a complicated tributary flow system (e.g. Stenoien and Bentley, 2000, see also Fig. 3) exhibiting a wide range of flow velocities, making it an ideal test case. The implications of our results for the past of PIG are discussed in Section 4.2.

Fig. 3 presents the results from the quantitative mapping of internal layers using the continuity-index averaged over 100 traces (part a) and 1000 traces (part b). The smoothing over 100 traces is useful for identifying anomalies, while the smoothing over 1000 traces gives a clearer regional picture, hence the inclusion of both plots here. For comparison, a manual classification of internal layering for the same data is presented as an inset in Fig. 3b (cf. Karlsson et al., 2009). The agreement between the continuity-index and the manual classification is further explored in Fig. 4a showing the mean values (μ) of ψ with one standard deviation (σ) for the three manually classified layer types: Absent, discontinuous and continuous ($\mu_a \pm \sigma_a$,$\mu_d \pm \sigma_d$, $\mu_c \pm \sigma_c$). The continuity-index of the data classified as absent overlaps slightly with the discontinuous areas (15% of the areas classified as absent has $\psi > \mu_d - \sigma_d$) and has practically no overlap with the continuous areas (1.2% of the areas classified as absent has $\psi > \mu_c - \sigma_c$). The discontinuous and continuous areas are less distinctly different, but this is not unexpected as the distinction between the two classes can be very subtle even when manual classification is used.

There is a clear correspondence between patterns of internal layering and the present ice-flow regime as mapped with InSAR satellite measurements (from Rignot, 2006): fast ice stream flow areas (>200 m a^{-1}) contain few or no layers, while slow flow areas (<50 m a^{-1}) contain continuous layers (using velocity boundaries from Shepherd et al., 2002). Flow velocities between 50 m a^{-1} and 200 m a^{-1} are often found in the tributaries and will be referred to as tributary flow. Here the continuity-index primarily displays intermediate values. The distribution of the continuity-index for the upper and lower velocity boundaries is shown in Fig. 4b and a simple t-test shows that with a confidence level of 5% the distributions are significantly different.

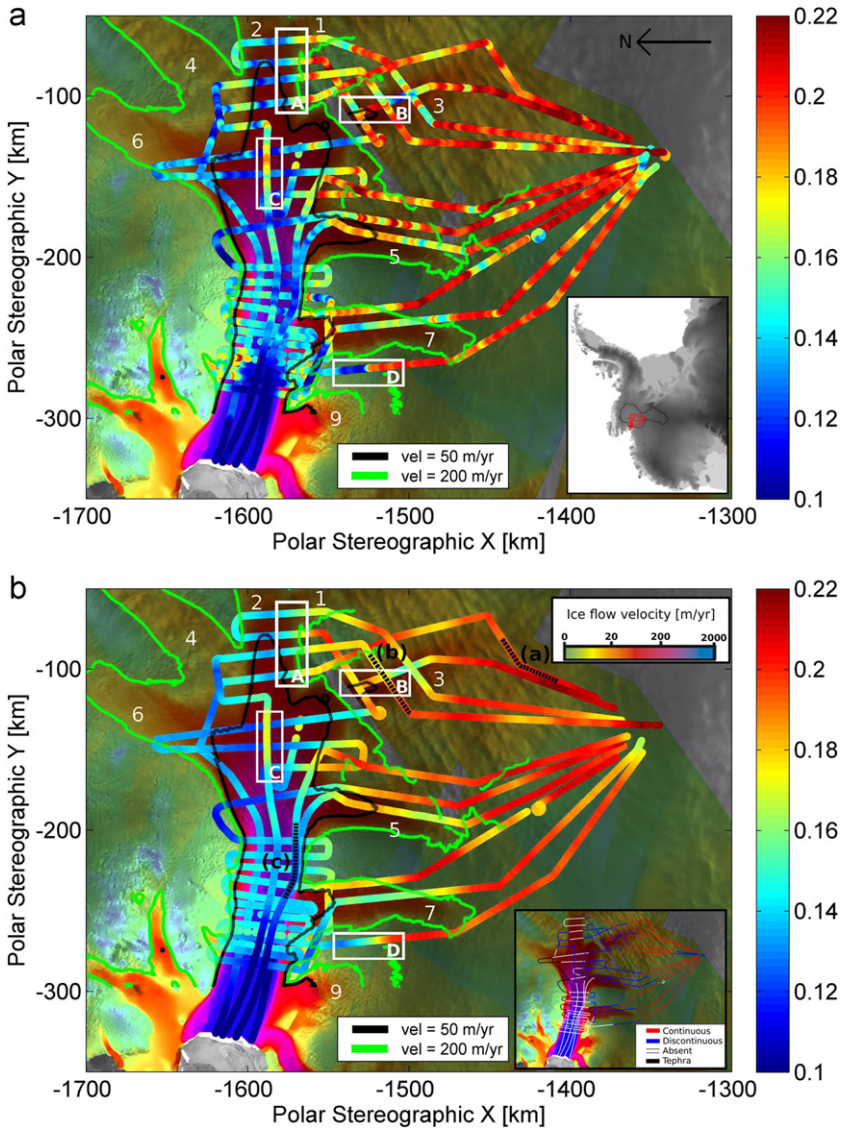

Fig. 3. Results from a quantitative analysis of several flightlines over PIG overlying InSAR measurements of surface velocities (Rignot, 2006) smoothed over (a) 100 traces and (b) 1000 traces, the inset shows the results from a manual analysis discussed in Karlsson et al. (2009). The 50 m a^{-1} and 200 m a^{-1} contours are shown with thick black and green lines respectively. The white boxes mark areas containing anomalous layering. Numbers in white refer to the tributaries following the scheme suggested by Stenoien and Bentley (2000). The location of the Z-scope images in Fig. 2 are marked with dashed black lines in (b).

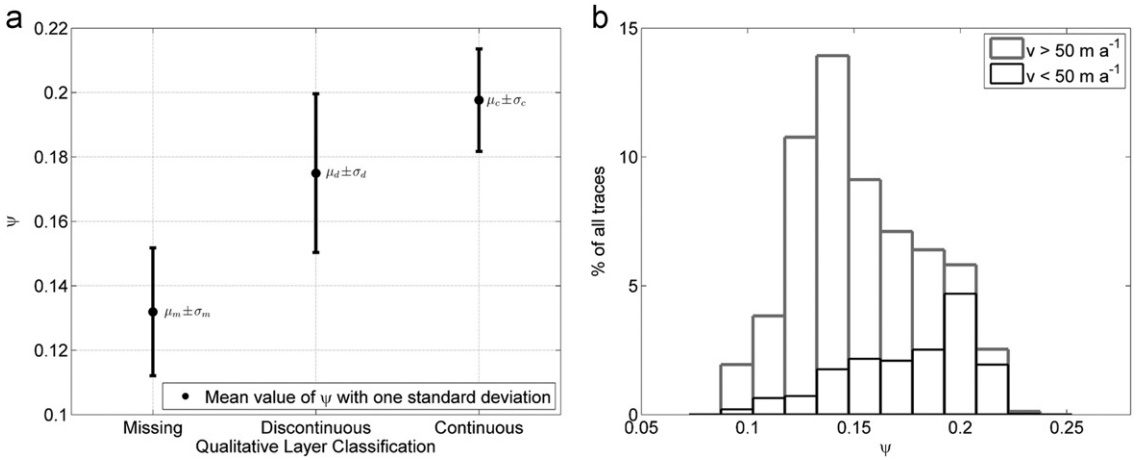

Fig. 4. (a) The mean of the continuity index for qualitatively distinguished absent, discontinuous and continuous layering with error bars showing one standard deviation. (b) Histogram of the continuity-index ψ from Fig. 3b for velocities above 50 m a^{-1} (grey) and below 50 m a^{-1} (black).

Areas of slow-flowing ice exhibit high continuity-indices (i.e. continuous and clear layering) with a mean value of 0.18, while areas of fast flow in the main trunk have low continuity-indices (few or absent layers) with a mean value of 0.14. Areas where flow transitions from slow to tributary and/or ice-stream flow occur are well associated with a corresponding change in continuity-index. In some areas the transition is very sharp, for example in the confluence of Tributary 1-2 (Fig. 3, Box A), where a qualitative change from discontinuous to absent layering at the tributary onset (and thus increasing flow rate) is matched by a distinct, sharp drop in continuity-index. In other areas (e.g. Tributary 5), the change in continuity-index is more gradual as the flightlines pass along the tributary and into the main trunk.

Two features particularly worthy of note are as follows. First, where flightlines intersect, continuity-indices are not always equal, and in some cases, are not even similar (e.g. boxes B and C, Fig. 3). Second, although the variations in continuity-index largely correspond with the spatial pattern of the current ice-flow regime, the correspondence is not perfect. For example, Box D in Fig. 3 shows low continuity-indices between 0.1 and 0.14 (discontinuous layering) in slow-flowing ice west of Tributary 7; and Box B and C indicate high continuity-indices between 0.18 and 0.2 (continuous layering) within Tributary 3 and the main trunk where ice flow exceeds 200 m a^{-1}. These instances counter the general findings, and possible reasons for their presence are discussed below.

4. Discussion

Our results have significance both in terms of outlining a quantitative, easily transferable method for the future analysis of RES-detected internal layering across other ice masses and for the information that variations in internal layers provide for interpreting the past flow of PIG. We now deal with each of these points in turn.

4.1. Methodological significance

We have presented a quantitative approach to studying isochrone geometries that requires minimal post-processing of the radar data and minimal interaction with users. It substantially reduces the time required to retrieve important information from RES dataset, is undertaken on a physically robust basis, and produces results over a continuous spectrum, rather than the tripartite scheme forced by manual methods (cf. Siegert et al., 2003; Rippin et al., 2006; Bingham et al., 2007). Importantly, the spatial patterns produced by our new quantitative technique regionally match those from the earlier manual classification method (Karlsson et al., 2009), and this reassures us that earlier layer-geometry mapping from other regions of Antarctica that relied on the manual technique (Siegert et al., 2003) remains valid. However, where digital RES data are available, it is clearly preferable to use a quantitative technique, not only to save data processing time but also to ensure internal consistency within the dataset and reproducibility in the layering classification results.

Other studies have also aimed at producing automatic methods for extracting information from internal layering, for example, Fahnestock et al. (2001), Sime et al. (2011) and Siegert et al. (2003). The former describes a method for tracing internal layers relying on initial user identification of a layer while Sime et al. (2011) use image processing with the aim of retrieving the slope of the isochrones. Both studies present powerful methods for comparison between radargrams and ice flow model outputs, but they rely on a large amount of user interaction (and thus subjectivity) and/or several data processing steps. Both methods also require post-processing of the data to increase the visibility of the layers and (in the case of Sime et al., 2011) tuning of the parameters to different types of radar data, both of which make for a more time consuming process. Finally, unlike the method described in this study they do not readily return a measure of the disruption of the internal layering. Siegert et al. (2003) attempted to extract information on internal layers by using spectral analysis. Although this approach successfully differentiated between continuous and discontinuous layers, it did not directly quantify the degree of layer disruption. It also relied on the fact that the internal layers already had been traced, which in and of itself is a very time consuming task. In contrast, while the quantitative method we present here does not contain information on the individual layer elevations or slopes, it has the basic advantage of requiring little dataset processing, i.e. it is simple and fast to apply to new RES data allowing for quick identification of areas of past change in flow regime.

As the amount of RES data increases, the development of a quantitative technique for classifying internal layers in radar data is a logical and necessary step forward. With a number of ice-sheet models now being developed to reproduce ice-flow fields from internal-layer architecture (Leysinger Vieli et al., 2007; Hindmarsh et al., 2009), our method offers a rapid and robust means of building up databases of internal-layer types across the major ice sheets against which such model output can be compared.

4.2. Internal layering in Pine Island Glacier

PIG is one of the largest and most rapidly changing glacial catchments in West Antarctica (Wingham et al., 2009). Satellite remote sensing over the past two decades has exposed unprecedented ice acceleration and ice-surface lowering across the catchment since observational records began (e.g. Rignot et al., 2008; Scott et al., 2009; Pritchard et al., 2009; Thomas et al., 2011). If this behavior continues, PIG will contribute significantly to 21st century global sea-level rise (Wingham et al., 2009). In order to assess its potential future rate of contribution to global sea level rise, it is critical to establish whether the currently observed changes represent a response to climate warming, or are part of longer-term natural fluctuations. It is hoped that this can ultimately be addressed with numerical modeling, and an essential question for model setup is whether the current spatial configuration of PIG's main trunk and tributaries has been stable or has been subject to major changes.

The internal layering observed in RES data is the result of the history of ice flow rates that the ice has been subjected to including both spatial and temporal patterns of ice flow. Thus a low continuity-index can result from a feature that is spatially stable but with changing ice flow rates in time or from changes in the spatial flow pattern. Based on this observation our results show that the geometry of the internal layers is, for the most part, consistent with that which we would expect from the current ice-flow regime, with regards to continuous layering/low disruption in slow flow areas outside the tributaries and main trunk, and greater disruption in the tributaries and main trunk. This is clearly demonstrated in Fig. 4b by the distribution of continuity indices for velocities above and below 50 m a^{-1}. While most of the continuity-indices from fast flow areas is less than 0.175 (gray histogram), the majority of continuity-indices for the slower flowing areas is larger than 0.175 (black histogram). Hence, our quantitative internal-layering analysis confirms that the main trunk and almost all of PIG's tributaries have remained in a spatially stable configuration for a period long preceding the onset of the currently observed dynamic thinning. This interpretation is consistent with the earlier finding that most of the tributaries and the main trunk lie within a network of deep subglacial troughs that serve to limit spatial migrations of the main tributaries (Vaughan et al., 2006). It also provides support

for the various inferences of measures of drag and basal roughness published recently that reinforced the spatial stability of the ice-stream and tributary configuration (Joughin et al., 2009; Morlighem et al., 2010; Rippin et al., 2011).

In order to estimate the duration of this apparently stable configuration we calculate the age of two deep isochrones using a simple relation between accumulation rate and age based on the Dansgaard–Johnsen model (Dansgaard and Johnsen, 1969)

$$t = \frac{2H-h}{2a} \ln\left(\frac{2H-h}{2z-h}\right), \quad h \le z \le H \tag{2}$$

where t is the time since deposition of the isochrone, H is the ice thickness, z is the depth of the isochrone, a is the accumulation rate and h is the so-called kink height (the height where the horizontal velocity is assumed to decrease linearly toward the bed). Eq. (2) is best suited for describing the age-depth relationship near an ice divide and depends on a good approximation of the value of h which is generally not known. Previous studies have used a value of $h = 400$ m for other parts of West Antarctica (Siegert and Payne, 2004) which we also apply here. Two flightlines with continuous layering are then selected, one in Tributary 3 and one close to the bottleneck between the northern and southern basin. Modern-day accumulation rates from Arthern et al. (2006) indicate an accumulation rate of approximately 0.5 m a^{-1} in the area. The two deepest visible isochrones then obtain an age of 7.2 ka (Tributary 3) and 18.6 ka (bottleneck). Changing the value of h to $h=0$ m (approximating a scenario where basal sliding is more important than ice deformation which is likely to be the case for Tributary 3) the ages then become 6.4 ka (Tributary 3) and 7.4 ka (bottleneck). Since accumulation rates in other parts of West Antarctica have been found to be equal to or lower than present day values in the past several thousand years (e.g. Siegert and Payne, 2004; Waddington et al., 2005) it is likely that the age of the isochrones is underestimated rather than overestimated. Geological records indicate that the ice shelf in front of PIG suffered a massive break-up towards the end of the Last Glacial Maximum and most likely over 12 ka ago (e.g. Lowe and Anderson, 2003; Jakobsson et al., 2011). Thus it would seem that the current stable configuration of the tributary system of PIG post-dates the ice shelf break-up while the inland configuration could be older. However, a better constraint on the age of the isochrones is needed to ascertain this with more certainty but that is beyond the scope of this study.

While our main conclusion is that the spatial distribution of PIG's flow is strongly dictated by its bed topography, implying long-term stability, there are a few areas (highlighted in Section 3 and boxed in Fig. 3) with anomalous continuity-indices that require clarification. In the area between Tributary 7 and Tributary 9 (Fig. 3, Box D), the continuity-indices are much smaller (<0.14, indicative of disrupted layering and enhanced/fast flow) than for other areas with similar, low flow velocities (typically $\psi \sim 0.18$). Comparison with the bed roughness in this area (see Fig. 4b in Rippin et al., 2011) shows no marked change in bed roughness. In earlier studies, buckled layering existing outside contemporary ice streams and tributaries has been interpreted as evidence of previous flow-feature migration (Rippin et al., 2003; Bingham et al., 2007). Tributary 7 is less topographically constrained than the other tributaries in PIG (Vaughan et al., 2006), and it would, therefore, be more vulnerable to lateral migration. We therefore suggest that the area west of Tributary 7 has experienced enhanced flow since the internal layers were deposited, either through the tributary being wider or through a change in its onset region.

The other most important anomalous result in Fig. 3 (Box C) is the existence of intermediate/high continuity-indices ($\psi \sim 0.17$ indicative of continuous layering and thus slow flow) within the main trunk of the ice stream where ice velocity approaches 1 km a^{-1}. However, Ng and Conway (2004) also noted the occurrence of continuous internal-layering along-flow within part of Kamb Ice Stream, where orthogonal radar lines exhibit clear buckling. They further showed that instances of continuous layering along-flow can be expected, but only where (i) the radar data have been collected in direct alignment with the main flowpath, and (ii) the actual position of the flow-feature has remained stable for a long period. Interpreted in this way, the pocket of high continuity-indices along flow in the central confluence zone of PIG is therefore not an anomaly but a result of a stable flow configuration, and further supports the longevity of the current spatial configuration. A similar phenomenon can be observed in Tributary 3 (Box B).

We therefore conclude that although the main trunk and tributaries of PIG have been experiencing dynamic thinning for at least the last 20 yr (Scott et al., 2009) and most likely for longer (Jenkins et al., 2010), the spatial configuration of the trunk and tributaries (with the possible exception of one tributary) is stable and is likely to remain so at present due to strong subglacial topographic control. Hence our internal-layering analysis, taken together with the previous studies of the nature of the basal boundary, suggests that ice-flow boundary conditions in numerical models of PIG do not need to take into account any major lateral migrations in the ice-flow fields across this catchment. We urge ice-sheet modelers to take this into consideration since it greatly reduces the complexity of the modeling approach required to simulate the future behavior of the PIG basin.

5. Conclusions

This paper has demonstrated the success of a quantitative layer classification scheme for the analysis of radio-echo sounding internal layers in ice sheets. The method presented here starts with raw trace data, does not rely on processing routines, and is independent of manual and/or qualitative assessments.

The method was applied to data from Pine Island Glacier and suggests long-term stability in the spatial configuration of the ice stream and its tributaries. This finding is consistent with the suggestion that PIG is topographically confined (Vaughan et al., 2006), and confirms that future numerical models of PIG can reasonably be set up using an ice-flow configuration similar to that seen today.

Finally, because the method works from raw-trace data, it is readily transferable to other ice-penetrating radar datasets from Antarctica and Greenland, providing an intuitive and fast method for classifying internal layering and thus assessing past and present flow dynamics. These datasets represent a vast archive of internal layers that, combined with developments in modeling internal-layering architecture, may hold the key to our understanding of the past and present development of ice sheets.

Acknowledgments

N.B. Karlsson was supported by a University of Hull scholarship. The work presented here was carried out in affiliation with the British Antarctic Survey and with additional support from the International Glaciological Society and the Anglo-Danish Society. The authors would like to thank H.F.J. Corr and acknowledge the logistical support for the field campaign of the British Antarctic Survey, The University of Texas and the US National Science Foundation. We thank the field party, and L. Byrne, who digitized the radar data. The authors would also like to acknowledge J. MacGregor and one anonymous reviewer whose comments significantly improved this manuscript.

References

Arthern, R.J., Winebrenner, D.P., Vaughan, D.G., 2006. Antarctic snow accumulation mapped using polarization of 4.3-cm wavelength microwave emission. J. Geophys. Res. 111, D06107.

Bingham, R.G., Siegert, M.J., Young, D.A., Blankenship, D.D., 2007. Organized flow from the South pole to the Filchner–Ronne ice shelf: an assessment of balance velocities in interior East Antarctica using radio echo sounding data. J. Geophys. Res. 112.

Catania, G., Conway, H., Raymond, C., Scambos, T., 2005. Surface morphology and internal layer stratigraphy in the downstream end of Kamb Ice Stream, West Antarctica. J. Glaciol. 51, 423–431.

Catania, G., Hulbe, C., Conway, H., 2010. Grounding-line basal melt rates determined using radar-derived internal stratigraphy. J. Glaciol. 56, 545–554.

Corr, H., Ferraccioli, F., Frearson, N., Jordan, T., Robinson, C., Armadillo, E., Caneva, G., Bozzo, E., Tabacco, I., 2007. Airborne radio-echo sounding of the Wilkes Subglacial Basin, the Transantarctic Mountains, and the Dome C region. Terra Ant. Rep. 13, 55–64.

Dansgaard, W., Johnsen, S., 1969. A flow model and a time scale for the ice core from Camp Century, Greenland. J. Glaciol. 8, 215–223.

Drewry, D.J., 1983. Antarctica: Glaciological and Geophysical Folio. Technical Report. University of Cambridge, Scott Polar Research Institute.

Drews, R., Eisen, O., Weikusat, I., Kipfstuhl, S., Lambrecht, A., Steinhage, D., Wilhelms, F., Miller, H., 2009. Layer disturbances and the radio-echo free zone in ice sheets. Cryosphere 3, 195–203.

Fahnestock, M., Abdalati, W., Luo, S., Gogineni, S., 2001. Internal layer tracing and age-depth-accumulation relationships for the northern Greenland ice sheet. J. Geophys. Res. 106, 33789–33797.

Fujita, S., Maeno, H., Uratsuka, S., Furukawa, T., Mae, S., Fujii, Y., Watanabe, O., 1999. Nature of radio echo layering in the Antarctic ice sheet detected by a two-frequency experiment. J. Geophys. Res. 104, 13013–13024.

Hindmarsh, R.C.A., Leysinger Vieli, G.J.M., Parrenin, F., 2009. A large-scale numerical model for computing isochrone geometry. Ann. Glaciol. 50, 130–140.

Hubbard, B., Glasser, N., 2005. Field Techniques in Glaciology and Glacial Geomorphology. John Wiley & Sons, Ltd, Chichester England.

Jacobel, R.W., Gades, A.M., Gottschling, D.L., Hodge, S.M., Wright, D.L., 1993. Interpretation of radar-detected internal layer folding in West Antarctic ice streams. J. Glaciol. 39, 528–537.

Jakobsson, M., Anderson, J.B., Nitsche, F.O., Dowdeswell, J.A., Gyllencreutz, R., Kirchner, N., Mohammad, R., O'Regan, M., Alley, R.B., Anandakrishnan, S., Eriksson, B., Kirshner, A., Fernandez, R., Stolldorf, T., Minzoni, R., Majewski, W., 2011. Geological record of ice shelf break-up and grounding line retreat, Pine Island Bay, West Antarctica. Geology 39, 691–694.

Jenkins, A., Dutrieux, P., Jacobs, S.S., McPhail, S.D., Perrett, A., White, D., 2010. Observations beneath Pine Island Glacier in West Antarctica and implications for its retreat. Nat. Geosci. 3, 468–472.

Joughin, I., Tulaczyk, S., Bamber, J.L., Blankenship, D., Holt, J.W., Scambos, T., Vaughan, D.G., 2009. Basal conditions for Pine Island and Thwaites Glaciers, West Antarctica, determined using satellite and airborne data. J. Glaciol. 55, 245–257.

Karlsson, N.B., Rippin, D.M., Vaughan, D.G., Corr, H.F.J., 2009. The internal layering of Pine Island Glacier, West Antarctica, from airborne radar-sounding data. Ann. Glaciol. 50, 141–146.

Leysinger Vieli, G.J.M.C., Hindmarsh, R.C.A., Siegert, M.J., 2007. Three-dimensional flow influences on radar layer stratigraphy. Ann. Glaciol. 46, 22–28.

Leysinger Vieli, G.M., Hindmarsh, R., Siegert, M., Bo, S., 2011. Time-dependence of the spatial pattern of accumulation rate in East Antarctica deduced from isochronic radar layers using a 3-D numerical ice flow model. J. Geophys. Res. 116.

Lowe, A.L., Anderson, J.B., 2003. Evidence for abundant subglacial meltwater beneath the paleo-ice sheet in Pine Island Bay, Antarctica. J. Glaciol. 49, 125–138.

Matsuoka, K., Furukawa, T., Fujita, S., Maeno, H., Uratsuka, S., Naruse, R., Watanabe, O., 2003. Crystal orientation fabrics within the Antarctic ice sheet revealed by a multipolarization plane and dual-frequency radar survey. J. Geophys. Res. 108.

Miners, W.D., Wolff, E.W., Moore, J.C., Jacobel, R., Hempel, L., 2002. Modeling the radio echo reflections inside the ice sheet at Summit, Greenland. J. Geophys. Res. 107.

Morlighem, M., Rignot, E., Seroussi, H., Larour, E., Dhia, H.B., Aubry, D., 2010. Spatial patterns of basal drag inferred using control methods from a full-Stokes and simpler models for Pine Island Glacier, West Antarctica. Geophys. Res. Lett. 37.

Ng, F., Conway, H., 2004. Fast-flow signature in the stagnated Kamb Ice Stream, West Antarctica. Geology 32, 481–484.

Pritchard, H.D., Arthern, R.J., Vaughan, D.G., Edwards, L.A., 2009. Extensive dynamic thinning on the margins of the Greenland and Antarctic ice sheets. Nature 46, 971–975.

Rignot, E., 2006. Changes in ice dynamics and mass balance of the Antarctic ice sheet. Philos. Trans. R. Soc., Ser. A 364, 1637–1655.

Rignot, E., Bamber, J.L., van den Broeke, M.R., Davis, C., Li, Y., van de Berg, W.J., van Meijgaard, E., 2008. Recent Antarctic ice mass loss from radar interferometry and regional climate modelling. Nat. Geosci. 1, 106–110.

Rippin, D.M., Siegert, M.J., Bamber, J.L., 2003. The englacial stratigraphy of Wilkes Land, East Antarctica, as revealed by internal radio-echo sounding layering, and its relationship with balance velocities. Ann. Glaciol. 30, 189–196.

Rippin, D.M., Siegert, M.J., Bamber, J.L., Vaughan, D.G., 2006. Switch-off of a major enhanced ice flow unit in East Antarctica. Geophys. Res. Lett. 30.

Rippin, D.M., Vaughan, D.G., Corr, H.F.J., 2011. The Basal Roughness of Pine Island Glacier, West Antarctica. J. Glaciol. 57, 67–76.

Scott, J.B.T., Gudmundsson, G.H., Smith, A.M., Bingham, R.G., Pritchard, H.D., Vaughan, D.G., 2009. Increased rate of acceleration on Pine Island Glacier strongly coupled to changes in gravitational driving stress. Cryosphere 3, 125–131.

Shepherd, A., Wingham, D.J., Mansley, J.A.D., 2002. Inland thinning of the Amundsen Sea sector, West Antarctica. Geophys. Res. Lett. 29.

Siegert, M.J., 1999. On the origin, nature and uses of Antarctic ice-sheet radio-echo layering. Prog. Phys. Geogr. 23, 159–179.

Siegert, M.J., Payne, A.J., 2004. Past rates of accumulation in central West Antarctica. Geophys. Res. Lett. 31.

Siegert, M.J., Payne, A.J., Joughin, I., 2003. Spatial stability of Ice Stream D and its tributaries, West Antarctica, revealed by radio-echo sounding and interferometry. Ann. Glaciol. 37, 377–382.

Sime, L.C., Hindmarsh, R.C.A., Corr, H.F.J., 2011. Automated processing of internal ice layer dips in radio-echo soundings. J. Glaciol. 57, 260–266.

Stenoien, M.D., Bentley, C.R., 2000. Pine Island Glacier, Antarctica: a study of the catchment using interferometric synthetic aperture radar measurements and radar altimetry. J. Geophys. Res. 105, 21761–21779.

Thomas, R., Frederick, E., Li, J., Krabill, W., Manizade, S., Paden, J., Sonntag, J., Swift, R., Yungel, J., 2011. Accelerating ice loss from the fastest Greenland and Antarctic glaciers. Geophys. Res. Lett. 38.

Vaughan, D.G., Corr, H.F.J., Ferracioli, F., Frearson, N., O'Hare, A., Mach, D., Holt, J.W., Blankenship, D.D., Morse, D.L., Young, D.A., 2006. New boundary conditions for the West Antarctic ice sheet: subglacial topography beneath Pine Island Glacier. Geophys. Res. Lett. 30.

Waddington, E.D., Conway, H., Steig, E.J., Alley, R.B., Brook, E.J., Taylor, K.C., White, J.W.C., 2005. Decoding the dipstick: thickness of Siple Dome, West Antarctica, at the last glacial maximum. Geology 33, 281–284.

Wingham, D.J., Wallis, D.W., Shepherd, A., 2009. Spatial and temporal evolution of Pine Island Glacier thinning, 1995–2006. Geophys. Res. Lett. 36.